Microfluid Nanofluid
DOI 10.1007/s10404-009-0483-9

RESEARCH PAPER

Realistic Brownian Dynamics simulations of biological molecule separation in nanofluidic devices

Ghassan N. Fayad · Nicolas G. Hadjiconstantinou

Received: 1 May 2009 / Accepted: 6 July 2009

Abstract We present a Brownian Dynamics model of biological molecule separation in periodic nanofilter arrays. The biological molecules are modeled using the Worm-Like-Chain model with Hydrodynamic Interactions. We focus on short dsDNA molecules; this places the separation process either in the Ogston sieving regime or the transition region between Ogston sieving and entropic trapping. Our simulation results are validated using the experimental results of Fu et al. (Phys Rev Lett 97:018103, 2006); particular attention is paid to the model's ability to quantitatively capture experimental results using realistic values of all physical parameters. Our simulation results showed that molecule mobility is sensitive to the device geometry. Moreover, our model is used for validating the theoretical prediction of Li et al. (Anal Bioanal Chem 394:427–435, 2009) who proposed a separation process featuring an asymmetric device and an electric field of alternating polarity. Good agreement is found between our simulation results and the predictions of the theoretical model of Li et al.

Keywords Molecular separation · DNA · Worm-Like chain · Brownian Dynamics · Hydrodynamic Interactions · Ogston sieving

1 Introduction

In this article we focus on the development of a Brownian Dynamics (BD) (Grassia et al. 1995; Öttinger 1996; Klenin et al. 1998) simulation framework for modeling the performance of nanofluidic separation devices. In particular, we are interested in the separation of short, $L \leq 900$ bp (324 nm), dsDNA molecules using nanofilter arrays (Fu et al. 2006, 2005); the latter are replacing traditional molecular sieving approaches for biological molecule separation (e.g., gel electrophoresis; Viovy 2000), and are of considerable importance to the chemical and pharmaceutical industry (Smejkal and Lazarev 2006; Giddings 1965; Scopes 1994). The ultimate goal of this research is the development of robust simulation methods which can replace costly experimental setups for device design and optimization.

The nanofilter device studied here consists of a large number ($N_p \sim 10{,}000$) of alternating shallow and deep regions etched in a silicon wafer as shown in Fig. 1. Biological molecules (DNA, protein) of contour length, L, persistence length, L_p and radius of gyration, R_g, driven by an electric field through this periodic array of constrictions are size-separated because their size-dependent mobilities result in size-dependent travel times. Typical (Fu et al. 2006) dimensions for the shallow and deep region depths and period are $d_s \approx 55$ nm, $d_d \approx 300$ nm, and $p \approx 1$ μm, respectively. This places the separation process in the Ogston regime (where the primary sieving mechanism derives from the steric hindrance due to the restriction) or the early transition region between the Ogston regime and entropic trapping (Fu et al. 2006).

Theoretical modeling of this process is very desirable for gaining fundamental understanding, device optimization, and parameter exploration (Laachi et al. 2007; Streek et al. 2004; Kim et al. 2004). Despite their small sizes, these devices contain a very large number of solvent molecules making classical molecular dynamics simulations intractable. In other words, for an efficient model, some degree of coarse-graining is required. In this study we

G. N. Fayad · N. G. Hadjiconstantinou (✉)
Mechanical Engineering Department,
Massachusetts Institute of Technology,
Cambridge, MA 02139, USA
e-mail: ngh@mit.edu

Published online: 29 July 2009

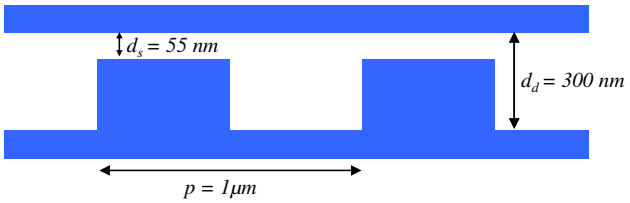

Fig. 1 Schematic of the nanofilter array

show that for the short molecules studied here, our Brownian Dynamics (BD) formulation strikes a good balance between fidelity—e.g., agreement with experimental data—and computational efficiency [compared to more expensive coarse-grained techniques such as Dissipative Particle Dynamics (Duong-Hong et al. 2008)].

Although BD simulations of biological molecule separation have appeared in the literature before (Streek et al. 2004; Panwar and Kumar 2006), those studies have focused on molecules that are sufficiently longer than L_p. In this limit the separation mechanism is different from Ogston sieving and is known as entropic trapping (Fu et al. 2006); moreover, as a result of the significantly larger molecule length, the Brownian Dynamics models were of the freely-jointed bead-spring type. A Brownian Dynamics study of short rod-like molecules in the geometry studied here has appeared recently (Laachi et al. 2007); however, the focus of that article was to demonstrate the feasibility of high-field electrophoresis and to highlight the importance of "torque assisted escape" in the latter limit.

Our objective is to construct a sufficiently realistic and efficient model that can *quantitatively* describe experimental data that are relevant to current engineering practice (low-field). Our preliminary study (see below) has verified that a rigid-rod model (Tao et al. 2005) cannot provide satisfactory agreement with experimental data for $L \gtrsim 2L_p$. As a result, this study utilizes the Worm-Like-Chain (WLC) model (Klenin et al. 1998; Allison 1986; Lewis et al. 1988) which includes the effects of bending and stretching stiffness. Our implementation of the WLC model is in line with the studies of Allison et al. (1986), Hagerman and Zimm (1981), Lewis et al. (1988), Klenin et al. (1998), and is thus different from Bead-Spring models that are usually used for long molecules (Öttinger 1996; Somasi et al. 2002).

The resulting Brownian Dynamics formulation includes hydrodynamic interactions between beads, and closely models the experimental set up of Fu et al. (2006) whose data are used for validation.

2 The WLC model

In typical WLC treatments (Klenin et al. 1998), the molecule is modeled as an elastic chain consisting of N beads of radius a connected by $N-1$ elastic links of average length L_0 as shown in Fig. 2. The chain conformation is specified by the locations $\mathbf{r}_i$, where $i = 1, \ldots, N$ of the N beads comprising the chain.

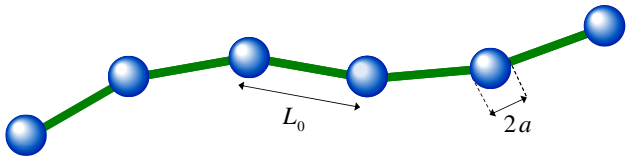

Fig. 2 DNA discretization into $N-1$ links and N beads

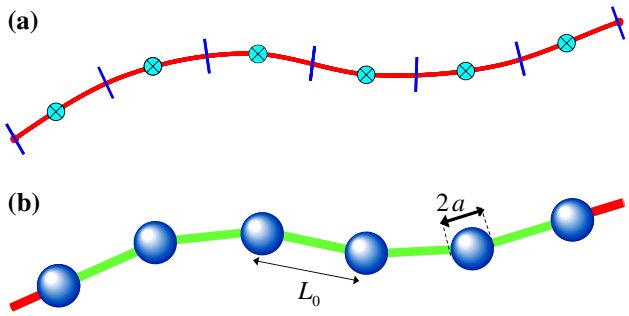

Fig. 3 DNA molecule discretization used in this study. **a** DNA molecule divided into N segments with N beads, **b** Beads are connected by $N-1$ elastic links

In the present study we use a slightly modified discretization which features N beads and N segments, as shown in Fig. 3. In this discretization, each bead represents the same fraction of chain length and hence makes the application of a common bead size and effective charge more justified. The beads are connected by $N-1$ elastic links (see Fig. 3). The half segments on each end of the molecule are assumed to be an extension of their nearest link, and are used in defining the molecule shape, e.g., during boundary condition imposition.

Our numerical formulation otherwise follows the study of Klenin et al. (1998); the chain elasticity includes stretching and bending contributions.

2.1 Numerical integration algorithm

The equation of motion (Klenin et al. 1998; Ermak and McCammon 1978) of each bead is integrated using the two-step algorithm of Klenin et al. (1998). In the first step we calculate a "predicted" displacement from

$$\mathbf{r}_i'(t+\Delta t) = \mathbf{r}_i(t) + \sum_{j=1}^{N} \mathbf{D}_{ij}(t) \frac{\mathbf{F}_j(t)}{k_B T} \Delta t + \mathbf{R}_i, \quad i = 1, \ldots, N \qquad (1)$$

where Δt is the time step and $\mathbf{F}_j(t)$ denotes the force on bead j; this force includes contributions from the externally applied electric field, as well as intra-bead forces which account for DNA stretching and bending resistance (Klenin et al. 1998). Here $\mathbf{D}_{ij}(t)$ denotes the diffusion interaction

tensor between beads i and j, which accounts for hydrodynamic interactions between these two beads; this is further discussed in Sect. 2.2. Finally, k_B is Boltzmann's constant and T is the simulation temperature. As implied by the notation, $\mathbf{D}_{ij}(t)$ and $\mathbf{F}_j(t)$ are calculated from the conformation $\{\mathbf{r}_i(t),\ i = 1,\ldots,N\}$ corresponding to time t.

The electrostatic force is calculated based on the bead effective charge and the electric field due to the externally applied voltage difference across the device (ΔV). The electric field is pre-computed on a triangular grid with maximum edge size of approximately 2 nm assuming insulating boundary conditions at the walls using the MATLAB *Partial Differential Equation Toolbox*. An approximation to this solution is stored on a square grid for quick access; each square has a side of 5 nm. The piece-wise constant electric field value associated with every square is the average value over all triangle centroids within the square. Note that due to the extremely fine initial triangular grid (more than 10^5 elements) and the very fine square "interpolation" grid (more than 10,000 squares) the error associated with this approximation is negligible compared to the modeling approximations and experimental uncertainties involved.

The random displacements $\mathbf{R}_i$ are defined by

$$\langle \mathbf{R}_i \rangle = 0 \tag{2}$$

$$\langle \mathbf{R}_i \otimes \mathbf{R}_j \rangle = 2\mathbf{D}_{ij}\Delta t \tag{3}$$

and can be calculated from a weighted sum of normal random deviates (Klenin et al. 1998; Ermak and McCammon 1978). Following the recommendation of Klenin et al., the diffusion tensor is updated every 10 time steps thus reducing the number of times the expensive factorization needs to be performed.

Finally, the second integration step is

$$\mathbf{r}_i(t+\Delta t) = \mathbf{r}_i'(t+\Delta t) + \sum_{j=1}^{N} \mathbf{D}_{ij}(t)\frac{\mathbf{F}_j'(t+\Delta t) - \mathbf{F}_j(t)}{k_B T}\Delta t, \quad i = 1,\ldots,N \tag{4}$$

where $\mathbf{F}_j'(t+\Delta t)$ are the forces calculated from the conformation $\{\mathbf{r}_i'(t+\Delta t), i = 1,\ldots,N\}$.

2.2 Hydrodynamic interactions

Hydrodynamic interactions between the beads are accounted for using the Rotne–Prager tensor (Rotne and Prager 1969):

$$\begin{aligned}
&\mathbf{D}_{ij} = D_0\mathbf{I} \qquad if \quad i = j \\
&\mathbf{D}_{ij} = D_0\frac{3a}{4r_{ij}}\left[\mathbf{I} + \frac{\mathbf{r}_{ij}\otimes\mathbf{r}_{ij}}{r_{ij}^2} + \frac{2a^2}{3r_{ij}^2}\left(\mathbf{I} - 3\frac{\mathbf{r}_{ij}\otimes\mathbf{r}_{ij}}{r_{ij}^2}\right)\right] \\
&\qquad if \quad r_{ij} \geq 2a, \quad i \neq j \\
&\mathbf{D}_{ij} = D_0\left[\left(1 - \frac{9}{32}\frac{r_{ij}}{a}\right)\mathbf{I} + \frac{3}{32}\frac{\mathbf{r}_{ij}\otimes\mathbf{r}_{ij}}{a r_{ij}}\right] \\
&\qquad if \quad r_{ij} \leq 2a, \quad i \neq j
\end{aligned} \tag{5}$$

where $D_0 = k_B T/6\pi\eta a$, η is the solvent viscosity, $\mathbf{r}_{ij} = \mathbf{r}_j - \mathbf{r}_i$, $r_{ij} = |\mathbf{r}_{ij}|$, $\mathbf{I}$ is the unity tensor, and $\mathbf{r}\otimes\mathbf{r}$ denotes the dyadic product.

The bead radius is chosen such that a reference DNA chain—a chain of contour length equal to one persistence length—has the desired diffusion coefficient. This is further discussed in Sect. 3.

2.3 Boundary conditions

Interactions with the walls are steric; in other words, if during a move, part of the molecule extends beyond one of the system boundaries, the move is rejected. In such a case, the molecule is assigned its original position, and a new step is taken which is again checked for boundary crossing. We have considered both including and neglecting the time increment during rejected moves; the difference to our results is negligible due to the small time step used which results in a number of rejected steps that is less than 1% of the total number of steps. Several researchers (Laachi et al. 2007; Panwar and Kumar 2006) have used similar boundary conditions. Reflecting boundary conditions, whereby a molecule (or parts of a molecule) is returned to the domain by taking the mirror image of the "offending" move, have also been used in some studies (Kim et al. 2004).

3 Simulation parameters

In accordance with the experiments of Fu et al. (2006), we consider dsDNA molecules of lengths $20.25\,\text{nm} \leq L \leq 324\,\text{nm}$ in a Tris–Borate–EDTA 5× buffer which diminishes the effect of electro-osmotic flow (Han and Craighead 2002). We consider average electric fields $E_{\text{av}} = \Delta V/(pN_p)$ in the range 20−400 V/cm.

The bending rigidity parameter in our model is chosen in such a way that the mean-square end-to-end distance of the dsDNA molecule equals that predicted by the Kratky–Porod (Kratky and Porod 1949; Marko and Siggia 1995) model.

$$\langle R^2 \rangle = 2L_p L\left[1 - \frac{L_p}{L}\left(1 - e^{-L/L_p}\right)\right] \tag{6}$$

Here the dsDNA persistence length was taken to be $L_p = 54$ nm (Fu et al. 2006; Lu et al. 2002).

The viscosity of the solvent (water) is taken to be 1.18×10^{-3} Pa s following the recent experimental results of Hsieh et al. (2008) for the buffer considered here.

The timestep was 10^{-8} s. This value was chosen such that all guidelines set by Klenin et al. (1998) are satisfied. The total simulated time modeling the experiments of Fu

et al. varied between 15 and 60 min (depending on the molecule length and electric field), and was such that the molecule traverses at least 10,000 periods. We have also verified that the initial position and configuration of the DNA molecule does not affect our results. In fact, to make sure that no "initial condition" effects are present, we start collecting data on the distance traveled by the molecule after 10^8 timesteps of relaxation (no field) and 10^8 timesteps of motion under the action of the electric field. The statistical uncertainty in the majority of our calculations is less than 1%, leading to error bars that are smaller than the symbols on the graph. Error bars are given when the statistical uncertainty is sufficiently large for the error bars to be visible.

Although it would have been desirable to use the same discretization (e.g., same discretization length L_0) for all molecules studied here, the range of lengths studied makes this impractical. In the interest of computational efficiency, the degree of coarse-graining increases in three steps: for $20.25\,\text{nm} \le L \le 54\,\text{nm}$ we use $L_0 = 6.75$ nm; for $54\,\text{nm} \le L \le 108\,\text{nm}$ we use $L_0 = 13.5$ nm; for $108\,\text{nm} \le L \le 324\,\text{nm}$ we use $L_0 = 27$ nm. Our simulation method becomes inefficient for significantly longer molecules, primarily due to the hydrodynamic interactions.

In view of the above steps in discretization, special attention was paid to ensure that the molecule drag (and diffusion coefficient) remains a smooth and continuous function of the molecule length. This was achieved (see Fig. 4) by using a different bead diameter for different discretizations. Given that the bead size remains constant for the same discretization, fixing the bead size for one "reference" molecule uniquely determines the bead size of all molecules. Here, the bead size of the reference dsDNA molecule ($L = 54$ nm, $L_0 = 13.5$ nm) was chosen such that the simulated diffusion coefficient $\hat{D}(L = 54\,\text{nm})$ of this molecule in water (viscosity 1×10^{-3} Pa s) matches the corresponding experimental result of Lukacs et al. (2000) who performed experiments for short dsDNA ($7\text{ nm} < L < 2{,}040$ nm) diffusing in water.

Using this procedure, our simulations yield a diffusion coefficient $\hat{D}(L)$ which is in excellent agreement with the experimental data fit as can be seen in Fig. 4. In fact, for molecules longer than 80 nm the resulting diffusion coefficient varies as $L^{-0.71}$, in excellent agreement with the exponent of Lukacs et al. (2000) (-0.72).

3.1 Modeling the free-draining mobility

Assuming a constant charge per unit length, q', the Nerst–Einstein relation (Pathria 1996)

$$\frac{\hat{D}}{\mu_{\text{NE}}} = \frac{k_B T}{q' L} \tag{7}$$

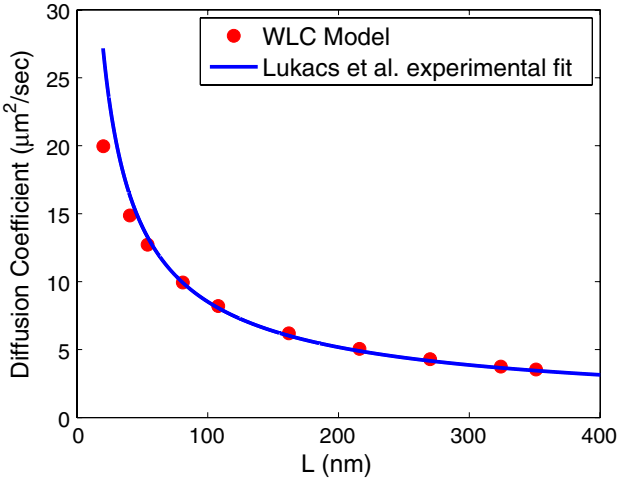

Fig. 4 Comparison between our simulation results and the experimental data of Lukacs et al. (2000) for the diffusion coefficient of dsDNA molecules in water

predicts that the Nerst–Einstein mobility scales with the molecule length according to $\mu_{\text{NE}} \propto L^{0.29}$.

However, as discussed extensively in the literature (Nkodo et al. 2001), in the presence of electric forces, hydrodynamic screening results in a free-solution mobility that is, to a very good approximation, independent of the dsDNA length (and different from the theoretically predicted μ_{NE}). This free-solution mobility will be denoted here by μ_{fs}.

Of particular interest are the careful experiments of Nkodo et al. (2001) which clearly show that while μ_{fs} is independent of the molecule length, the molecule diffusivity is unaffected by the electric field, exhibiting Zimm scaling for sufficiently long molecules (Nkodo et al. report an exponent ranging between -0.68 and -0.86 for short ssDNA molecules; this compares well with the value of -0.72 of Lukacs et al. and -0.71 found here for dsDNA molecules).

Developing a Brownian Dynamics model which captures these phenomena from first principles is very difficult. On the other hand, neglecting hydrodynamic interactions as in previous studies will result in a molecule diffusivity that scales as L^{-1}, which differs significantly from the expected behavior. This is particularly important in the present study where the translational Péclet number $Pe = q' L E_{\text{av}} d_s / k_B T$ ranges between 0.04 and 5, requiring accurate representation of the balance between diffusion and advection. As we show below, a nonlinear response to the electric field appears for $Pe \gtrsim 0.2$. for the device designed and tested by Fu et al.

To circumvent these difficulties we implemented a method which allows the free-draining behavior to be reproduced with minimal modification to the BD

algorithm, and virtually no effect on the diffusion coefficient. The method amounts to allowing the molecule effective charge per unit length to vary with L such that the observed (free-draining) mobility is independent of the molecule length. In other words we let $q'(L) = (L/L_p)^{-0.29} q'_{\mathrm{ref}}$ such that

$$\mu_{\mathrm{fs}} = \frac{q' L \hat{D}}{k_B T} \tag{8}$$

is independent of L. Note that because the variation of q' with L is dictated by the experimental data (Nkodo et al. 2001; Stellwagen et al. 1997) the only adjustable parameter in the model is the value of q'_{ref} which, due to the choice $q'(L = 54\,\mathrm{nm}) = q'_{\mathrm{ref}}$, can be thought of as the effective charge of the reference molecule; the value used for q'_{ref} in this study will be given in the next section. Moreover, due to its relatively weak dependence on L, q' varies by less than a factor of 3 over the range $20.25\,\mathrm{nm} \leq L \leq 324\,\mathrm{nm}$ studied here.

4 Simulation results

Our simulations suggest that the device geometry affects molecule transport significantly. For this reason, we have modeled the following two geometries:

1. Square-well geometry (Fig. 1) with dimensions d_s = 55 nm, $d_d = 300$ nm, $p = 1$ μm as given in (Fu et al. 2006).
2. Tapered geometry shown in Fig. 5. The shape of the transition from deep to shallow regions was transcribed from the SEM image of a similar device ($p = 2$ μm) shown in (Fu et al. 2006). The resulting model geometry is characterized by d_s = 55 nm, d_d = 300 nm, $p = 1$ μm, and a taper angle of 62°; the transition from the deep to the narrow region occurs in two steps as shown in Fig. 5.

These two geometries result in substantially different mobility levels (about 40%). For this reason, for each geometry the value of q'_{ref} was chosen such that the resulting mobility is in agreement with one reference experimental result ($L = 20.25$ nm, $E = 64.3$ V/cm). The resulting values of q'_{ref} are $5.9 \times 10^{-11}\,\frac{C}{m}$ for case 1 and $4.3 \times 10^{-11}\,\frac{C}{m}$ for case 2. The value of effective charge, especially for the more realistic case 2, compares very favorably with the value given by Smith and Bendich (1990) ($4.45 \times 10^{-11}\,\frac{C}{m}$)

Figure 6 shows a comparison between our simulation results for the two geometries shown in Figs. 1 and 5 and the experimental results of Fu et al. In addition to a significantly different mobility level, our model shows that the two geometries result in different molecule selectivity.

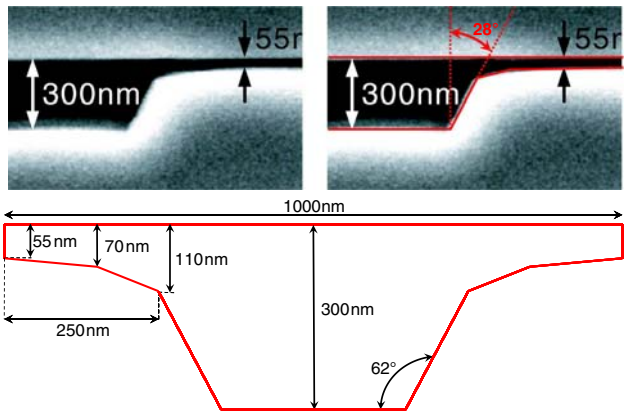

Fig. 5 SEM image and more realistic geometry

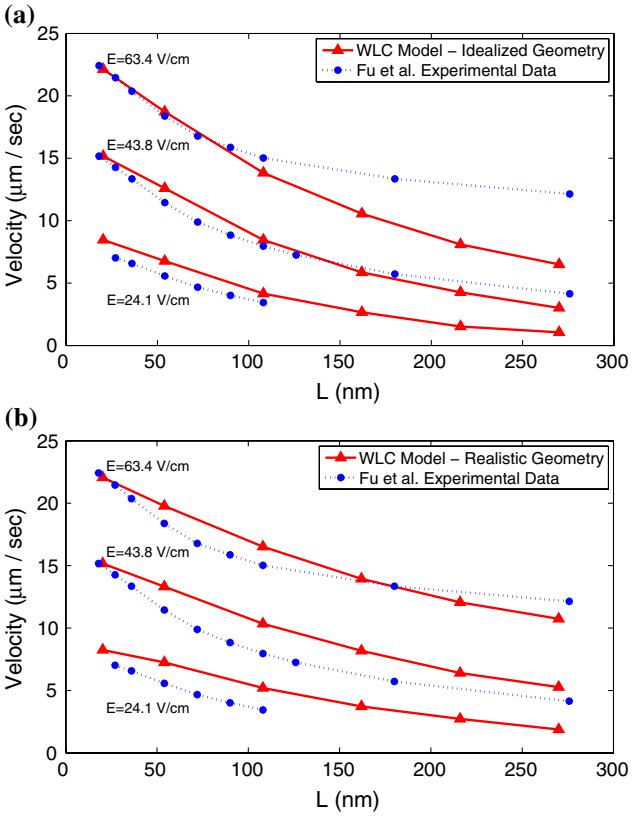

Fig. 6 Simulation results for different geometries. **a** Comparison with experimental results for the idealized geometry of Fig. 1, **b** comparison with experimental results for the more realistic geometry of Fig. 5

Although the tapered geometry results in inferior selectivity, not surprisingly, it is in better *overall* agreement with the experimental results of Fu et al., compared to the idealized geometry. Our results also show that for the realistic geometry of Fig. 6, the molecule mobility increases non-linearly with increasing electric field for $Pe \gtrsim 0.2$.

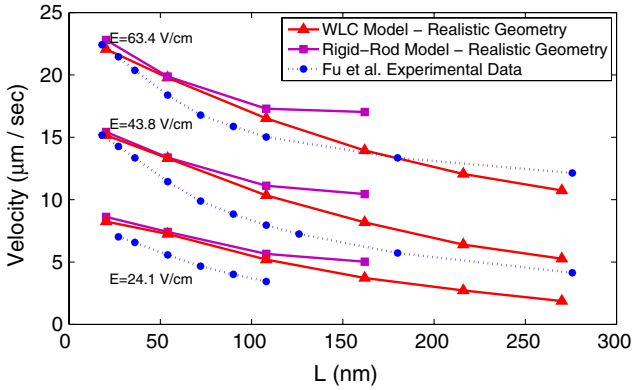

Fig. 7 Comparison between WLC and rigid-rod model results (realistic geometry)

4.1 Comparison with a rigid-rod model

During our preliminary study, we investigated the range of applicability of the rigid-rod model. Figure 7 shows a comparison between the rigid-rod and WLC results for the more realistic geometry. The rigid-rod results were obtained using the algorithm described in (Tao et al. 2005), while physical parameters were chosen such that the two models have equivalent charge per unit length and drag. As, expected, the rigid-rod and WLC models are in very good agreement for $L \lesssim 100$ nm ($\simeq 2L_p$). The error for $L \approx 100$ nm is of the order of 10% and increases as L increases. This is in agreement with the observation of Fu et al. (2006).

4.2 Molecular probability distribution

Although the Brownian Dynamics method is inherently stochastic and yields noisy results, characterization of the complete molecule probability distribution is feasible and not very computationally intensive. The plots shown here are obtained by discretizing the simulation domain into small cells and recording the relative frequency of occupation by the mid-point of the molecule. These results are plotted in the figure as two-dimensional contour plots as well as one-dimensional density plots as a function of the device length; the latter are obtained by integrating the two-dimensional density in the direction normal to the direction of travel.

These plots can be very useful for obtaining a qualitative understanding of the device operation. For example, the comparison of Figs. 8 and 9 can be used to investigate the origin of the effects of geometry on molecule mobility observed in Fig. 6. Figures 8 and 9 show that more time is spent in the deep region (and in particular, trying to enter the shallow region) of the *idealized* geometry compared to the more *realistic* geometry, suggesting that the effect of the geometry on the effective energy barrier contributes to the mobility difference significantly. Note that these plots

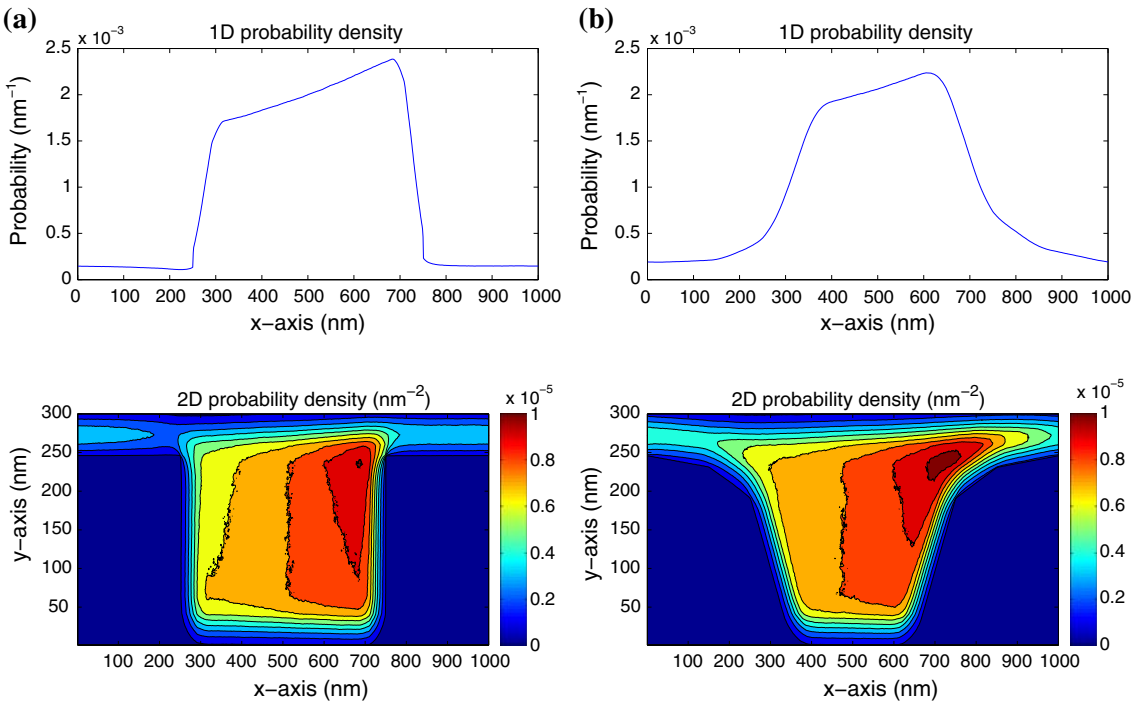

Fig. 8 Probability density distribution for L = 108 nm, E_{av} = 63.4 V/cm. **a** Idealized geometry, **b** realistic geometry

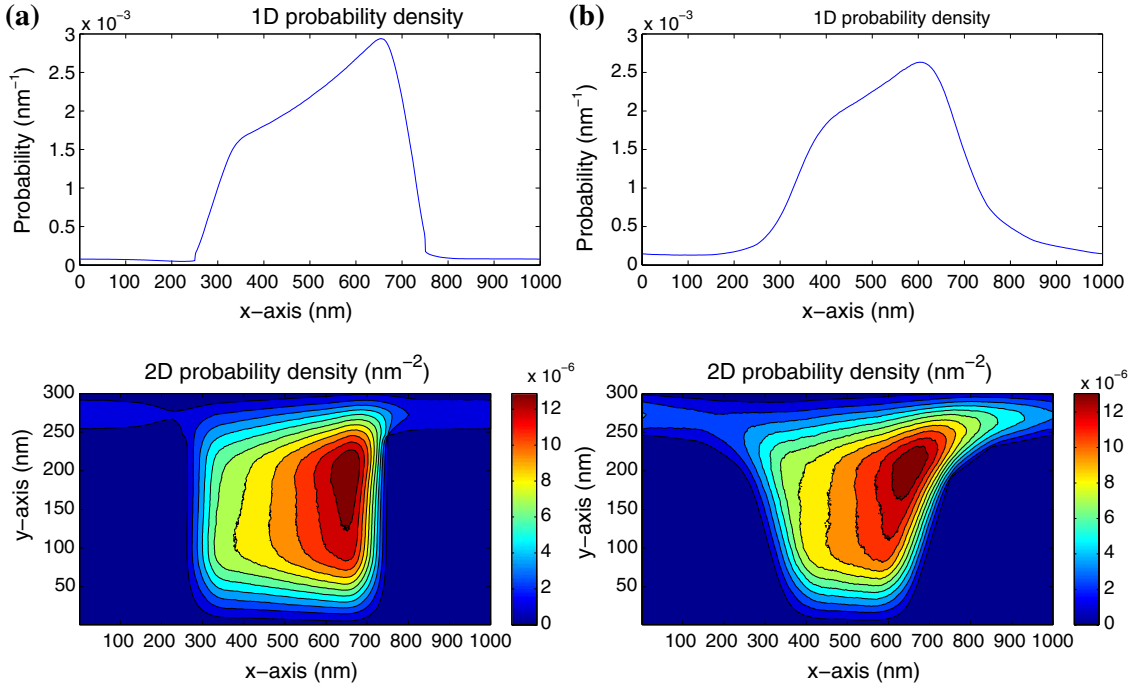

Fig. 9 Probability density distribution for $L =$ 216 nm, E_{av} = 63.4 V/cm. **a** Idealized geometry, **b** realistic geometry

were generated with the same q'_{ref} (namely $q'_{ref} = 4.3\times 10^{-11}\frac{C}{m}$) to ensure that the increased q'_{ref} in the idealized geometry is not the reason for the observed discrepancy.

5 Separation using asymmetric devices

In this section we discuss simulations of electrophoretic motion in asymmetric devices. This study is motivated by recent theoretical results (Li et al. 2009) suggesting that comparable separation using a significantly shorter device can be achieved using asymmetric devices (see Fig. 10) in conjunction with an electric field of alternating polarity. This proposal is based on the observation that the asymmetry in the device geometry will result in different mobilities in the two directions of travel which can be explored using an alternating electric field, to yield a macroscopic drift. In particular, the device shown in Fig. 10 uses the observation that a slanted wall reduces the entropic barrier for travel in one direction significantly while leaving the entropic barrier for travel in the other direction essentially unchanged. The model of Li et al. (2009) treats DNA molecules as rigid rods and models them as point particles by accounting for their orientational configurations and resulting steric hindrance using a local partition coefficient. Assuming absence of torques due to electrostatic effects, and dominant diffusion, a one-dimensional advection–diffusion equation is formulated and numerically solved. The assumption of dominant diffusion also requires (Li et al. 2009) that the characteristic time associated with the voltage oscillation period is long compared to the time taken for traversing one geometrical period.

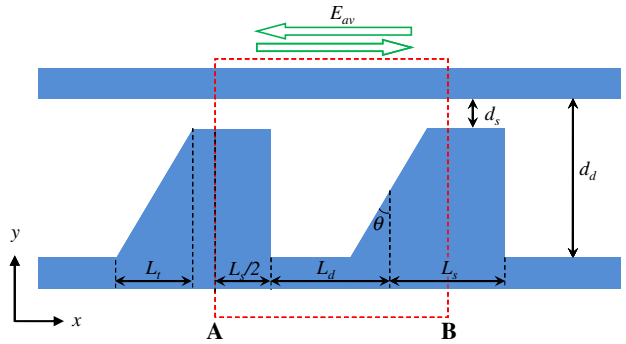

Fig. 10 Schematic of one period of the asymmetric nanofilter array

To validate the main theoretical prediction of Li et al. but also investigate how a more realistic representation (e.g., finite chain stiffness, three-dimensional geometry, significantly longer molecules) modifies their results, we performed Brownian Dynamics simulations using the model described above. We focus on the case $\theta = \pi/4$ with $d_s = 60$ nm, $d_d = 240$ nm, $L_s = L_d = 500$ nm. Results for the net molecule velocity for three electric field strengths (100, 200, and 400 V/cm) are shown in Fig. 11. For the results shown here, the electric field is of the form of a square wave of frequency $f = 0.1$ Hz. Other simulations, not shown here, have established that, as expected, the net

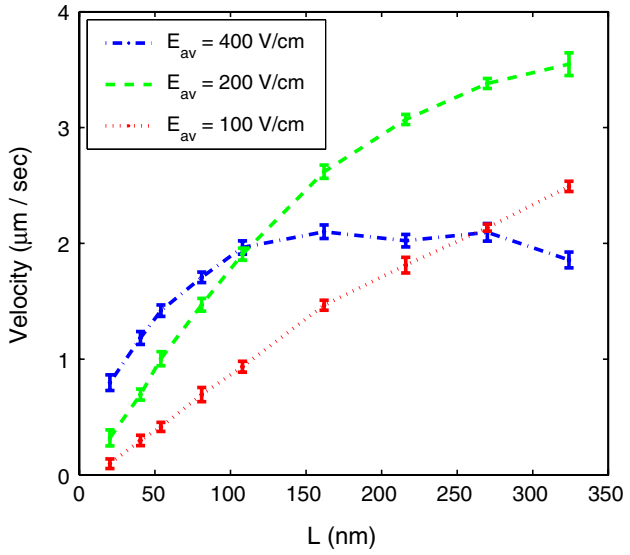

Fig. 11 Net velocity of dsDNA molecules of different lengths in asymmetric device under AC fields of varied strength

molecule velocity is independent of the oscillation frequency, provided that $1/f$ is long compared to the time taken by the molecule to traverse one geometric period (p). The results support the main conclusion of Li et al., namely that asymmetry can be exploited to achieve separation. Our model also shows that the molecule mobility appears to increase monotonically with molecule length well beyond the rigid-rod regime. Saturation is visible for long molecules/high electric fields; in fact, it appears that the controlling variable is the product of E and L, or in other words Pe. Our results suggest that saturation occurs for $Pe \gtrsim 1.5$.

Figure 12 shows the probability density of the DNA molecule (L = 270 nm, E_{av} = 100 V/cm, and Pe = 0.99) as it is traveling through the asymmetric channel under the action of an AC field. As expected, the figure shows that molecules spend a longer time trying to enter the narrow region when traveling to the left than when traveling to the right.

6 Discussion

We have presented an efficient BD model of electrophoretic short-dsDNA-molecule separation in nanofluidic devices. Our results show that both the separation efficiency and molecule mobility are sensitive to the device geometry, with the latter exhibiting a difference of the order of 40% between the idealized and a more realistic geometry. The model achieves good agreement with the experimental results of Fu et al. using only one adjustable parameter. A more accurate comparison with experimental data requires a more precise characterization of the *actual*

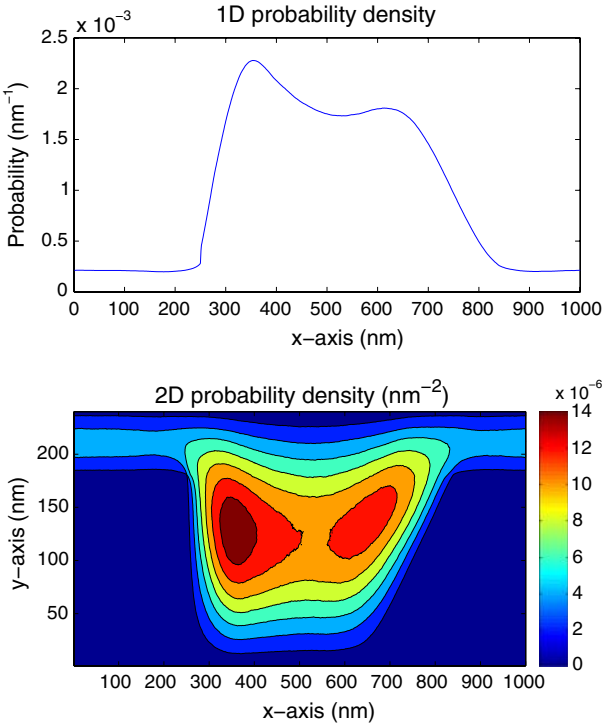

Fig. 12 Probability density distribution in asymmetric channel with AC field for L = 270 nm, E_{av} = 100 V/cm (Pe = 0.99)

system geometry and the associated variability between different periods, as well as more accurate characterization of other system parameters (e.g., electric field strength, electroosmotic flow magnitude).

The mobility differences between the two geometries studied here are in line with the conclusions of previous theoretical treatment of rigid rod molecules (Li et al. 2009) which shows that wall tapering increases molecule mobility, both in an absolute sense but also as a function of molecule length, with longer molecules experiencing a larger increase in mobility. For the conditions studied in (Li et al. 2009) (short molecules and low to medium electric field) this behavior was primarily attributed to the reduction of the effective energy barrier as a result of the tapered geometry.

Simulations in asymmetric devices in the presence of an electric field of alternating polarity show a monotonic increase of molecule mobility with molecule length, essentially verifying the prediction by Li et al. (Li et al. 2009) for short molecules. Saturation and thus loss of selectivity is observed for $Pe \gtrsim 1.5$.

It is noteworthy that reasonable agreement with experimental data for $L < 100$ nm ($\simeq 2L_p$) can be obtained using rigid-rod BD simulations. This observation is consistent with previous study (Li et al. 2008) based on a continuum transport model which utilizes the statistical theory of Giddings to characterize the entropic barrier; the latter

study also finds that for $L < 100$ nm agreement with the experimental results of Fu et al. is good but for $L \approx 100$ nm some discrepancy is visible.

The model presented here is sufficiently accurate to be useful for the design of new separation devices as well as evaluation and optimization of newly proposed devices; one example of the latter is a device featuring a two-dimensional geometry to achieve continuous separation (Fu et al. 2007).

Acknowledgments The authors are grateful to Professor J. Han and his group (Dr. Jianping Fu in particular), for making their experimental data available and for useful discussions. This study was supported by the Singapore-MIT alliance (SMA-II, CE program).

References

Allison SA (1986) Brownian Dynamics simulation of wormlike chains—fluorescence depolarization and depolarized light-scattering. Macromolecules 19(1):118–124

Duong-Hong D, Han J, Wang J, Hadjiconstantinou NG, Chen YZ, Liu G (2008) Realistic simulations of combined DNA electrophoretic flow and eof in nano-fluidic devices. Electrophoresis 29(24):4880–4886

Ermak DL, McCammon JA (1978) Brownian Dynamics with hydrodynamic interactions. J Chem Phys 69(4):1352–1360

Fu J, Mao P, Han J (2005) Nanofilter array chip for fast gel-free biomolecule separation. Appl Phys Lett 87(26):263902

Fu J, Yoo J, Han J (2006) Molecular sieving in periodic free-energy landscapes created by patterned nanofilter arrays. Phys Rev Lett 97(1):018103

Fu J, Schoch RB, Stevens AL, Tannenbaum SR, Han J (2007) A patterned anisotropic nanofluidic sieving structure for continuous-flow separation of DNA and proteins. Nat Nanotechnol 2:121–128

Giddings JC (1965) Dynamics of chromatography. Part 1. Principles and theory. Marcel Dekker, New York

Grassia PS, Hinch EJ, Nitsche LC (1995) Computer-simulations of Brownian-Motion of complex-systems. J Fluid Mech 282:373–403

Hagerman PJ, Zimm BH (1981) Monte carlo approach to the analysis of the rotational diffusion of wormlike chains. Biopolymers 20(7):1481–1502

Han J, Craighead HG (2002) Characterization and optimization of an entropic trap for DNA separation. Anal Chem 74(2):394–401

Hsieh C, Balducci A, Doyle PS (2008) Ionic effects on the equilibrium dynamics of DNA confined in nanoslits. Nano Lett 8(6):1683–1688

Kim SH, Panwar AS, Kumar S, Ahn KH, Lee SJ (2004) Electrophoresis of a bead–rod chain through a narrow slit: a Brownian Dynamics study. J Chem Phys 121(18):9116–9122

Klenin K, Merlitz H, Langowski J (1998) A Brownian Dynamics program for the simulation of linear and circular DNA and other wormlike chain polyelectrolytes. Biophys J 74(2):780–788

Kratky O, Porod G (1949) Röntgenuntersuchung gelöster fadenmoleküle. Recueil des Travaux Chimiques des Pays-Bas-Journal of the Royal Netherlands Chemical Society 68(12):1106–1122

Laachi N, Declet C, Matson C, Dorfman KD (2007) Nonequilibrium transport of rigid macromolecules in periodically constricted geometries. Phys Rev Lett 98(9):098106

Lewis RJ, Allison SA, Eden D, Pecora R (1988) Brownian Dynamics simulations of a three-subunit and a ten-subunit worm-like chain: comparison of results with trumbell theory and with experimental results from DNA. J Chem Phys 89(4):2490–2503

Li ZR, Liu GR, Chen YZ, Wang J, Bow H, Cheng Y, Han J (2008) Continuum transport model of ogston sieving in patterned nanofilter arrays for separation of rod-like biomolecules. Electrophoresis 29(2):329–339

Li ZR, Liu GR, Han J, Chen YZ, Wang J, Hadjiconstantinou NG (2009) Transport of biomolecules in asymmetric nanofilter arrays. Anal Bioanal Chem 394(2):427–435

Lu Y, Weers B, Stellwagen NC (2002) DNA persistence length revisited. Biopolymers 61(4):261–275

Lukacs GL, Haggie P, Seksek O, Lechardeur D, Freedman N, Verkman AS (2000) Size-dependent DNA mobility in cytoplasm and nucleus. J Biol Chem 275(3):1625–1629

Marko JF, Siggia ED (1995) Stretching DNA. Macromolecules 28(26):8759–8770

Nkodo AE, Garnier JM, Tinland B, Ren H, Desruisseaux C, McCormick LC, Drouin G, Slater GW (2001) Diffusion coefficient of DNA molecules during free solution electrophoresis. Electophoresis 22(12):2424–2432

Öttinger HC (1996) Stochastic processes in polymeric fluids: tools and examples for developing simulation algorithms. Springer, Berlin, New York

Panwar AS, Kumar S (2006) Time scales in polymer electrophoresis through narrow constrictions: a Brownian Dynamics study. Macromolecules 39(3):1279–1289

Pathria RK (1996) Statistical mechanics, 2nd edn. Butterworth-Heinemann, Boston

Rotne J, Prager S (1969) Variational treatment of hydrodynamic interaction in polymers. J Chem Phys 50(11):4831–4837

Scopes RK (1994) Protein purification: principles and practice. Springer, New York

Smejkal GB, Lazarev A (eds) (2006) Separation methods in proteomics. CRC Taylor & Francis, Boca Raton, FL

Smith SB, Bendich AJ (1990) Electrophoretic charge density and persistence length of DNA as measured by fluorescence microscopy. Biopolymers 29(8–9):1167–1173

Somasi M, Khomami B, Woo NJ, Hur JS, Shaqfeh ESG (2055) Brownian Dynamics simulations of bead–rod and bead–spring chains: numerical algorithms and coarse-graining issues. J Non-Newton Fluid Mech 108(1–3):227–255

Stellwagen NC, Gelfi C, Righetti PG (1997) The free solution mobility of DNA. Biopolymers 42(6):687–703

Streek M, Schmid F, Duong TT, Ros A (2004) Mechanisms of DNA separation in entropic trap arrays: a Brownian Dynamics simulation. J Biotechnol 112(1–2):79–89

Tao Y, Den Otter WK, Padding JT, Dhont JKG, Briels WJ (2005) Brownian Dynamics simulations of the self- and collective rotational diffusion coefficients of rigid long thin rods. J Chem Phys 122(24):244903

Viovy J (2000) Electrophoresis of DNA and other polyelectrolytes: physical mechanisms. Rev Mod Phys 72(3):813–872